ISSN 0030-400X, Optics and Spectroscopy, 2010, Vol. 108, No. 5, pp. 685–692. © Pleiades Publishing, Ltd., 2010.
Original Russian Text © G. Hakhumyan, D. Sarkisyan, A. Sargsyan, A. Atvars, M. Auzinsh, 2010, published in Optika i Spektroskopiya, 2010, Vol. 108, No. 5, pp. 727–734.

SPECTROSCOPY OF ATOMS AND MOLECULES

Investigation of Rb D_1 Atomic Lines in Strong Magnetic Fields by Fluorescence from a Half-Wave-Thick Cell

G. Hakhumyan[a], D. Sarkisyan[a], A. Sargsyan[a], A. Atvars[b], and M. Auzinsh[b]

[a] *Institute of Physical Research, Armenian National Academy of Sciences, Ashtarak-0203, Armenia*

[b] *Department of Physics, Latvian University, Riga, LV-1586 Latvia*

Received October 2, 2009

Abstract—It has been experimentally demonstrated that the use of the effect of significant narrowing of the fluorescence spectrum from a nanocell that contains a column of atomic Rb vapor with a thickness of $L = 0.5\lambda$ (where $\lambda = 794$ nm is the wavelength of laser radiation, whose frequency is resonant with the atomic transition of the D_1 line of Rb) and the application of narrowband diode lasers allow the spectral separation and investigation of changes in probabilities of optical atomic transitions between levels of the hyperfine structure of the D_1 line of ^{87}Rb and ^{85}Rb atoms in external magnetic fields of 10–2500 Gs (for example, for one of transitions, the probability increases ~17 times). Small column thicknesses (~390 nm) allow the application of permanent magnets, which facilitates significantly the creation of strong magnetic fields. Experimental results are in a good agreement with the theoretical values. The advantages of this method over other existing methods are noted. The results obtained show that a magnetometer with a local spatial resolution of ~390 nm can be created based on a nanocell with the column thickness $L = 0.5\lambda$. This result is important for mapping strongly inhomogeneous magnetic fields.

DOI: 10.1134/S0030400X10050048

INTRODUCTION

Many optical and magnetic processes that take place upon the interaction of narrowband laser radiation with atomic vapors have found use in laser technology and metrology, the production of high-sensitivity magnetometers, quantum communications, information storage, and so on [1, 2]. This creates a great deal of interest in these investigations.

It is well-known that atomic transitions of alkali metals split in magnetic fields into Zeeman components, whose frequency shifts deviate from the linear behavior in already moderate magnetic fields. As this takes place, the probabilities of atomic transitions usually change significantly as well [3, 4]. It was demonstrated in [5, 6] that the use of resonance fluorescence spectra of a nanocell filled with atomic vapor and having a thickness of $L = 0.5\lambda$ (where $\lambda = 794$ nm is the wavelength of laser radiation whose frequency is resonant to the atomic transition of the D_1 line of Rb) allows one to separate and study the atomic transitions between the levels of the hyperfine structure of the D_1 line of ^{87}Rb atoms in magnetic fields with $B = 10$–200 Gs. The achieved high sub-Doppler spectral resolution is caused by the effect of a strong narrowing of the fluorescence spectrum of a nanocell with the atomic vapor column thickness $L = 0.5\lambda$ (the method was called FHL) compared to normal 1-cm-long cells (for which the Doppler width is ~500 MHz). With the proper choice of parameters, it is possible to achieve a sevenfold narrowing of the spectrum. In [7, 8], the D_2 lines of Rb and Cs atoms were studied by the FHL method in fields ~50 Gs.

It is known that, with the saturated absorption (SA) technique, the sub-Doppler spectral resolution can also be achieved using centimeter-long cells (when the parameters are properly chosen, it is possible to obtain peaks of reduced absorption with a width close to the natural width of ~6 MHz). In [9, 10], the SA technique was used to study spectra of the D_1 and D_2 lines of Rb atoms. One of significant disadvantages of the application of the SA technique is the presence of so-called cross-over resonances in spectra. In the magnetic field, these resonances split into numerous components, making the spectrum extremely difficult to process. This restricts the magnitude of acceptable magnetic fields and, as a rule, B should be below 100 Gs. Another significant disadvantage is the fact that the SA is strongly nonlinear and, therefore, the peak amplitudes of the decreased absorption do not correspond to probabilities of atomic transitions at whose frequencies these peaks are formed. This additionally complicates the processing of the spectra. At the same time, using the FHL technique, the peak value of fluorescence (up to laser intensities of several tens of milliwatts per square centimeter) corresponds to probabilities of atomic transitions [11]. This allows one to directly study the dependence of the probabilities on B. Another important advantage of the FHL method is the possibility of using strong permanent

magnets (PMs) that can generate fields of several thousand Gs at distances of several centimeters. The fields of these PMs are strongly nonuniform and the gradient can achieve ~100–200 Gs/mm, which makes it impossible to use centimeter-long cells. At the same time, due to the small thickness of the nanocell (~400 nm), the gradient of B in it is four to five orders of magnitude smaller than the measured value of B. This remarkable feature of a nanocell was used in the study of absorption spectra of atomic vapors in the fields ranging within 1–2400 Gs [12] at the vapor column thickness $L = \lambda$ (the method was called LZM).

The aim of this work was to experimentally demonstrate that the FHL technique at magnetic fields of 0–2500 Gs can have advantages over the LZM. In the first turn, FHL provides a better signal-to-noise contrast, which makes it possible to record and study even weak atomic transitions. The spectrum in FHL is formed on a horizontal straight line, whereas, in the LZM technique, peaks of decreased absorption are superimposed on the absorption spectra, which complicates the processing of results. In addition, since, in FHL, the thickness of the vapor column is twice as small as that in LZM, the spatial resolution is doubled, which is important for the mapping of strongly inhomogeneous magnetic fields.

EXPERIMENTAL

Nanocell Design

The design of the nanocell is similar to that described in [11, 13]. To successfully implement the FHL technique, a region of a homogeneous thickness with a relatively large area equal to the laser beam cross section (~4 mm^2) is necessary. This is achieved through the sputtering of an ~600-nm-thick Al_2O_3 layer in the form of a 10-mm-long, 1-mm-wide stripe on the bottom part of one of the nanocell windows. 20×30-mm rectangular nanocell windows with thicknesses of 3 mm are made of nonbirefringent crystalline garnet ($Y_5Al_5O_{12}$). In addition, the garnet is resistant to aggressive hot Rb vapor. The internal gap between the well-polished windows (better than $\lambda/10$) is slightly wedged. Due to the large size of the window, it is quite easy to form the region with the thickness $L = 0.5\lambda$.

Since the gap thickness (30 mm from the upper boundary to the lower one) changes by 600 nm, the behavior of the nanocell is close to the behavior of a low-Q Fabry–Perot interferometer. This allows one to determine the thickness L accurate to ~15 nm from the interference pattern of the reflected laser beam [11]. In particular, at the thickness $L = 0.5\lambda$ at $\lambda = 794$ nm, the zero reflection is observed. If the beam diameter exceeds the area in which $L = 0.5\lambda$, then a dark spot with a diameter equal to the zone in which $L = 0.5\lambda$ is formed against the background of the reflected beam.

The nanocell furnace is made of nonmagnetic materials and has three holes, two of which are designed to transmit the laser radiation and a side hole is meant for recording fluorescence. The furnace consists of two heaters, the first of which heats the window, and the second one is made as a sapphire sidearm containing the metal. The temperature of the top boundary of the metal Rb column (in the sapphire sidearm) was 120°C, which provided the vapor density $N \sim 2 \times 10^{13}$ cm^{-3}. To prevent the condensation of the Rb vapor on the nanocell windows, the window temperature was maintained at a level ~140°C.

Experimental Setup and Results

The experimental setup is shown schematically in Fig. 1a. Here, ECDL (extended cavity diode laser) is the continuous-wave diode laser with $\lambda = 794$ nm (for the narrowing of the lasing line. The ECDL employs the scheme with a diffraction grating, which allows the lasing line to be narrowed to ~1 MHz (tuning range of several tens of gigahertz)). FI is the Faraday insulator. A $\lambda/4$ plate (*1*; coated at $\lambda = 794$ nm) is used for obtaining circularly polarized pump radiation σ^+ (left circle) and σ^- (right circle). A disk PM (*2*; $\varnothing = 50$ mm and a thickness of ~8 mm) has a hole of $\varnothing = 2$ mm for the passage of the laser radiation (the PMs were fixed on two nonmagnetic tables with the gradually changeable separation). The nanocell (*3*) has the thickness of the Rb vapor column of $L = 0.5\lambda$. Photodetectors (*4*) were based on FD-24K photodiodes with a receiving aperture of ~1 cm^2 (the large aperture is important for the recording of weak fluorescence signals). The photodiode signal was amplified by an operational amplifier and arrived at a four-beam digital Tektronix TDS2014B oscilloscope (*5*). Part of the laser radiation was directed to the cell with Rb, in which the SA spectrum was formed, which served as a frequency reference for the spectra obtained with the nanocell at $L = 0.5\lambda$ in the external magnetic field. Magnetic studies were carried out in the configuration shown in Fig. 1b. The magnetic field **B** was directed along the direction z of the laser radiation propagation (**B** || **k**), and the fluorescence of the Rb vapor was recorded in the direction perpendicular to the direction of the laser radiation propagation. To obtain a minimal width of the fluorescence spectrum, it is important for the laser radiation to be directed perpendicularly to the nanocell windows [11]. If the laser radiation spot is shifted by 10–20% of 0.5λ (390 nm), this leads to only an additional broadening of the spectrum by roughly the same value; that is, the FHL method is not very critical to the parameter $L = 0.5\lambda$, which is important for its practical application. The furnace housing the nanocell was placed between two PMs (*2*), and as the separation between them changed, the value of B applied to the Rb vapor changed gradually (the magnetic field was measured by a calibrated magnetometer based on a Hall-effect sensor).

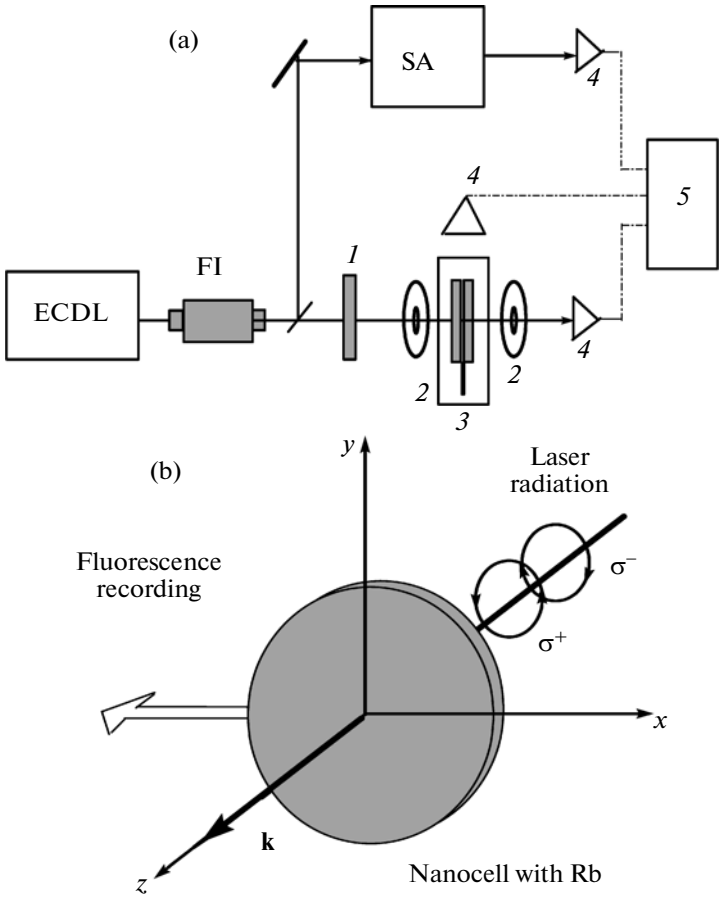

Fig. 1. (a) Optical layout of experimental setup: ECDL (extended cavity diode laser) is continuous-wave laser diode; (*1*) coated $\lambda/4$ plate; (*2*) constant magnets; (*3*) nanocell; (*4*) photodetectors; (*5*) Tektronix TDS2014B oscilloscope; (SA) unit for formation of spectrum based on the saturated absorption technique; (b) configuration of magnetic measurements.

Figure 2a (right part) shows the diagram for the D_1 line of ^{87,85}Rb upon circularly polarized σ^+ (left circle) laser excitation, which initiates the transitions between the magnetic sublevels m_F (^{87}Rb, $5S_{1/2}$, $F_g = 1 \rightarrow 5P_{1/2}$, $F_e = 1$, 2 and ^{85}Rb, $5S_{1/2}$, $F_g = 2 \rightarrow 5P_{1/2}$, $F_e = 2$, 3) with the selection rule $\Delta m_F = +1$. The power of the laser radiation was 2 mW at a beam diameter of 2 mm. Figure 2a shows the fluorescence spectra of the nanocell with $L = 0.5\lambda$ at different values of B (for convenience of comparison, the spectra are shifted along the vertical; the spectrum at $B = 0$ is shown in Fig. 2c): (I) 250, (II) 830, (III) 1350, (IV) 1875, and (V) 2500 Gs. At fields of up to 600 Gs, 14 components are easily recorded (the corresponding enumeration of the transitions is shown in Fig. 2a to the right). The transitions marked by the numbers *1*, *2*, *3*, *4*, *5*, *6*, *7*, and *8* are the strongest. Moreover, the amplitudes of these lines continue to increase as the magnetic field increases up to 2500 Gs (0.25 T). As can be seen, the transition $F_g = 1, m_F = +1 \rightarrow F_e = 2, m_F = +2$ of ^{87}Rb is convenient for determining the magnetic field because it has the highest amplitude (among the transitions *1*, *2*, and *3*) and does not overlap the other components at any B (according to the theory, there is no overlap with other components up to fields of 1 T). As for the transition $F_g = 1 \rightarrow F_e = 1$ of ^{87}Rb, which gives two components between Zeeman sublevels (in Fig. 2a at $B = 250$ Gs these transitions are marked by the numbers *1*' and *2*'), it does not appear in the experiment with $B > 1000$ Gs in fluorescence spectra (for the σ^+ radiation) because the probability of this transition vanishes fast as the magnetic field increases. The spectral width of fluorescence is 110–120 MHz, but it can be decreased to ~70 MHz with a more careful choice of parameters. The lower curve in Fig. 2a is the frequency reference obtained by the SA technique with the ordinary cell with Rb (frequency reference from [14]).

Figure 2b shows a fragment of the fluorescence spectrum (enclosed in the dash-and-dot rectangle in Fig. 2a) of the nanocell with $L = 0.5\lambda$ at $B = 250$ Gs for the transition $5S_{1/2}$, $F_g = 2 \rightarrow 5P_{1/2}$, $F_e = 2$, 3 of ^{85}Rb obtained at a slower scanning (the spectral resolution is better in this case). As can be seen from the

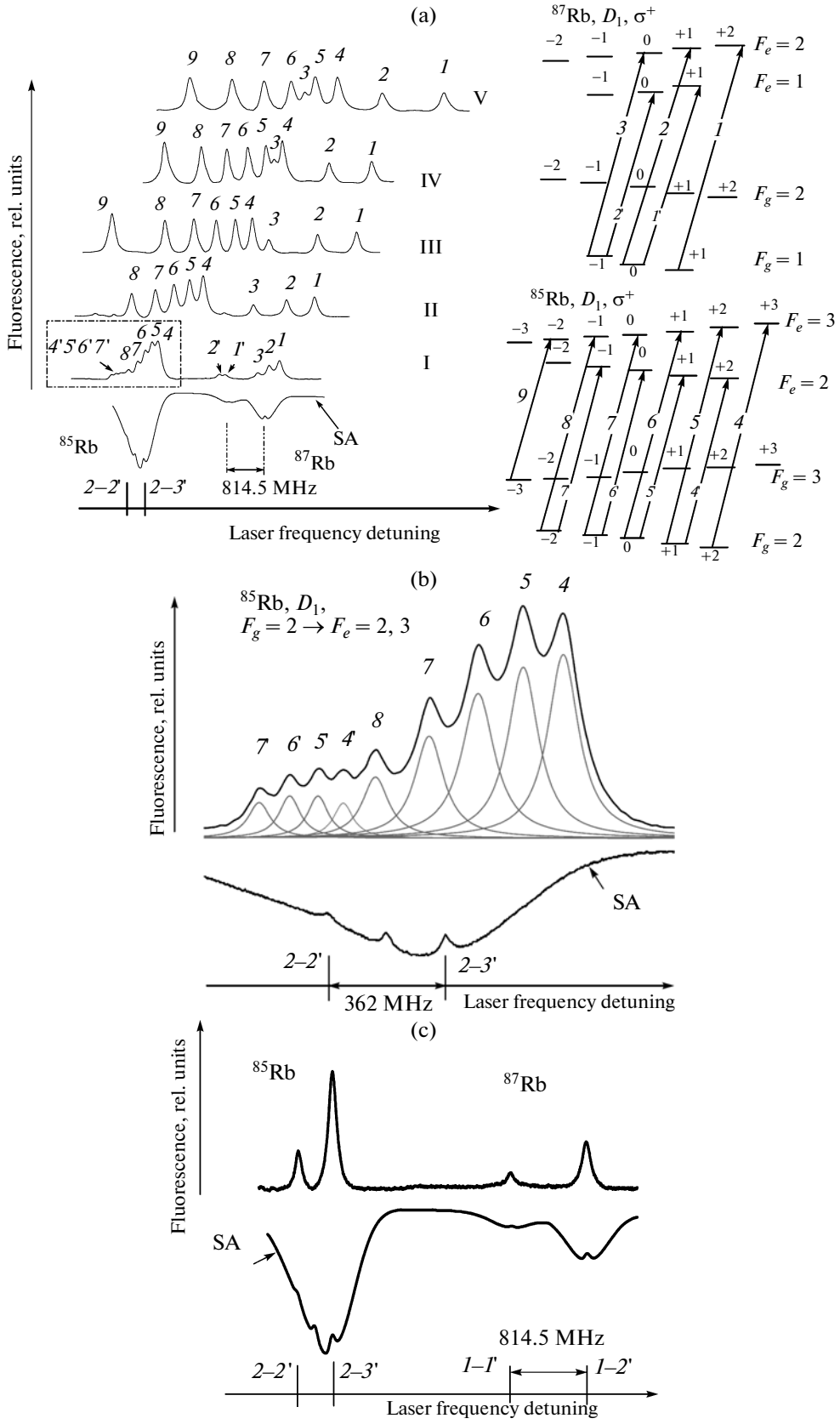
(a)
^{87}Rb, D_1, σ^+
$F_e = 2$
$F_e = 1$
$F_g = 2$
$F_g = 1$
^{85}Rb, D_1, σ^+
$F_e = 3$
$F_e = 2$
$F_g = 3$
$F_g = 2$
Fluorescence, rel. units
V
IV
III
II
I
^{85}Rb
^{87}Rb
SA
2–2'
2–3'
814.5 MHz
Laser frequency detuning
(b)
^{85}Rb, D_1,
$F_g = 2 \rightarrow F_e = 2, 3$
Fluorescence, rel. units
SA
2–2'
2–3'
362 MHz
Laser frequency detuning
(c)
^{85}Rb
^{87}Rb
Fluorescence, rel. units
SA
814.5 MHz
2–2'
2–3'
1–1'
1–2'
Laser frequency detuning

Fig. 2. (a) fluorescence spectrum of 390-nm-thick nanocell for B = (I) 250, (II) 830, (III) 1350, (IV) 1875, and (V) 2500 Gs (for convenience, the spectra are shifted along the vertical); numeration of ^{87}Rb and ^{85}Rb transitions, the D_1 line is shown to the right on the diagram of energy levels for the pumping by the σ^+ radiation. All 15 transitions shown in the diagram are resolved. The lower (reference) curve is the SA spectrum. (b) Fragment of the fluorescence spectrum (enclosed in the dot-and-dash rectangle in Fig. 2a) of the nanocell at $B = 250$ Gs for the ^{85}Rb transition $5S_{1/2}$, $F_g = 2 \rightarrow 5P_{1/2}$, $F_e = 2, 3$; all nine components are resolved. The envelope of the spectrum is approximated by 9 Lorentz curves (gray curves). The lower (reference) is the SA spectrum. (c) Fluorescence spectrum of the nanocell with $L = 0.5\lambda$ at $B = 0$ for the D_1 line of ^{85}Rb $F_g = 2 \rightarrow F_e = 2, 3$ and ^{87}Rb $F_g = 1 \rightarrow F_e = 1, 2$. The lower curve is the SA spectrum.

figure (the envelope of the spectrum is approximated by nine Lorentz curves (gray lines)), all nine components are spectrally resolved. At $B = 0$, the probability ratios (in relative units) for transitions *4*, *5*, *6*, *7*, and *8* for the σ^+ transitions are 15 : 10 : 6 : 3 : 1. It is interesting to note that the probability of transition *8* increases quickly with an increasing magnetic field and, already at low fields (~250 Gs), it is $A(4)/A(8) \approx 3$, whereas the initial ratio is $A(4)/A(8) = 15$ (at $B = 0$) (this is in agreement with the theoretical curves shown below). It should be also noted that, in the centimeter-long cell, the envelope of the fluorescence spectrum is fully smooth (no substructure). The lower curve is the frequency reference obtained by the SA technique.

It should be noted that the amplitudes of lines *4*, *5*, *6*, *7*, and *8* continue to increase, as the magnetic field increases up to 2500 Gs, whereas components *4'*, *5'*, *6'*, and *7'* (transitions $5S_{1/2}$, $F_g = 2 \rightarrow 5P_{1/2}$, $F_e = 2$ of ^{85}Rb) are already absent as in the experiment at $B >$ 1000 Gs because the probabilities of these transitions (for the σ^+ radiation) vanish fast with an increasing magnetic field. At $B = 0$, the probability ratios for transitions *4'*, *5'*, *6'*, and *7'* are 3 : 2 : 2 : 3. This ratio remains nearly unchanged at $B = 250$ Gs, but the transition probabilities decrease. It should be noted that, if an additional nanocell is used, the fluorescence spectrum at $B = 0$ can also serve as a good frequency reference (upper curve in Fig. 2c); the lower curve is the SA spectrum.

RESULTS AND DISCUSSION

The experiment was compared with the theoretical model. In the case of D_1 transitions in the gas of alkali metals, the nonlinear energy shift of magnetic sublevels in the constant magnetic field can be calculated by the Rabi–Breit method [15, 16]. We can find changes in the probabilities of optical transitions between magnetic sublevels, if the mixing coefficients of wave functions in the magnetic field are known. This mixing can be found by determining the eigenvectors of the perturbed Hamiltonian of the family of hyperfine atomic levels in the magnetic field [4, 17].

Figure 3a shows the frequency shift of components *1*, *2*, and *3* (relative to their initial position at $B = 0$), while Fig. 3b shows the frequency shift of components *4*, *5*, *6*, *7*, and *8*. The theoretical curves are shown by solid lines. One can see a good agreement with the experiment. It follows from Fig. 3a that the linear Zeeman effect for components *1* and *2* is observed up to $B \sim 500$ Gs, and their frequency shift is well described by the values of 1.16 and 0.93 MHz/Gs, respectively. At $B > 1000$ Gs, the tuning rate of component *1* (which is a good candidate for the measurement of external magnetic fields) is 1.59 MHz/Gs.

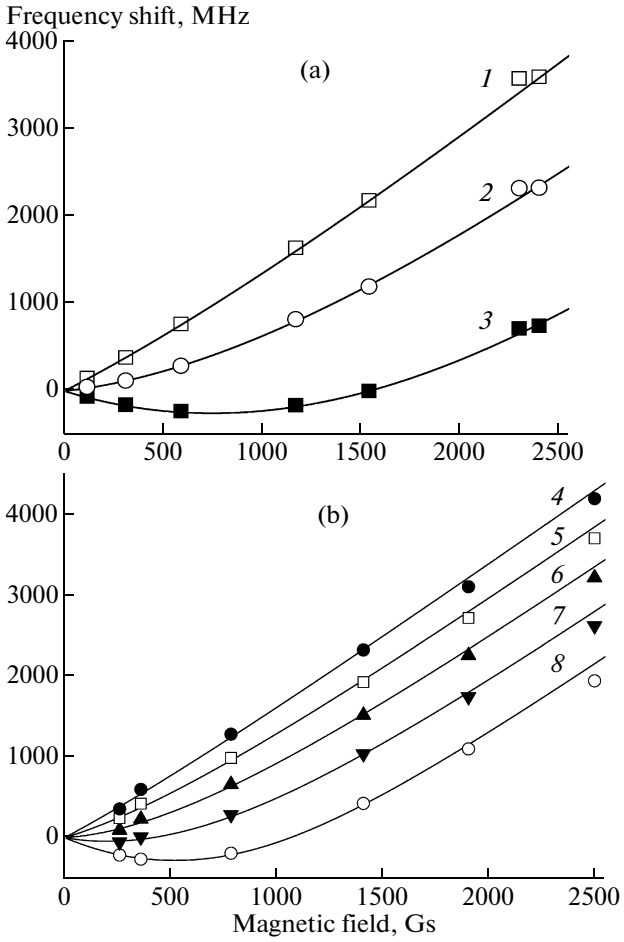

Fig. 3. (a) Frequency shift of components *1*, *2*, and *3* relative to the initial position at $B = 0$: (solid curves) theory. (b) Frequency shift of components *4*, *5*, *6*, *7*, and *8* relative to the initial position at $B = 0$: (solid curves) theory.

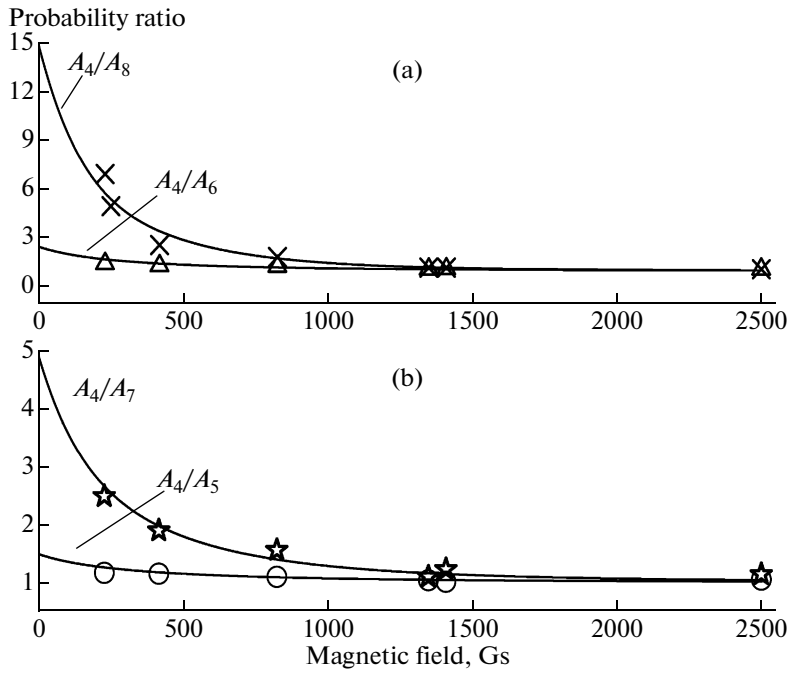

Fig. 4. (a) Probability ratios for transitions A_4/A_8 and A_4/A_6: (solid line) theory. (b) Probability ratios for the transitions A_4/A_7 and A_4/A_5: (solid line) theory. As magnetic field increases, probabilities of transitions *5*, *6*, *7*, *8* approach probability of transition *4* (which increases by a digit of 1.18 as the magnetic field increases from 0 to 2500 Gs).

At low magnetic fields, the probabilities of transitions *1*, *2*, *3* relate to one another as 6 : 3 : 1. However, as the magnetic field increases, the probabilities of transitions *2* and*3* approach the probability of transition *1* (as can be seen from Fig. 2a), which, in turn, increases by a factor of 1.25 as the magnetic field increases from 0 to 2500 Gs. At $B > 1200$ Gs, the tuning rates for components *4*, *5*, and *6* are roughly the same and equal to 1.71 MHz/Gs. It is interesting to note that, at fields $B > 1000$ Gs, the fluorescence peak of the transition $F_g = 3, m_F = -3 \rightarrow F_e = 3, m_F = -2$ of ^{85}Rb (marked by *9*) is observed in the spectrum in Fig. 2a. At $B = 0$ this peak is shifted by ~3 GHz relative to the initial position of components *4*, *5*, *6*, *7*, and *8*. This occurs due to the highest tuning rate of component *9* (1.85 MHz/Gs) among all the presented components. It should be noted that the probability of component *9* increases with the increase of the magnetic field, achieving the probability of component *4*. Both of these facts are also well confirmed by the theory.

It was noted above that at low magnetic fields the probabilities of transitions *4*, *5*, *6*, *7*, and *8* differ widely (the probability is maximal for transition *4*). However, as the magnetic field increases, the probabilities of transitions *5*, *6*, *7*, and *8* become nearly the same as the probability of transition *4* (it can be seen from Fig. 2a). Figures 4a and 4b show the probability ratios for transitions *5*, *6*, *7*, and *8* relative to transition *4*. Theoretical curves are shown by solid lines and good agreement is seen. It is interesting to note that, for transition *8*, the initial probability ratio is $A_4/A_8 = 15$. However, as the magnetic field increases from zero to 2500 Gs, this ratio approaches unity. Since, at high fields, the probability of transition *4* increases by a factor of 1.18, the final increase in the probability for transition *8* is ~17 times.

It should be noted that, in fields $B \sim 2500$ Gs, components *1* and *2* shift to the high-frequency region by 3856 and 2478 MHz, respectively, where there are no frequency references. The theoretical calculations show that, in fields $B \sim 5000$ Gs, the frequency shifts increase up to ~8 and 6.5 GHz, respectively, and the probabilities of these transitions increase as well. Therefore, the nanocell along with a pair of strong PMs can be a convenient and simple frequency reference for the high-frequency wing of ^{87}Rb.

Let us compare the method of investigation of atomic lines in strong magnetic fields (1–2400 Gs) with the aid of atomic absorption spectra at the vapor column thickness $L = \lambda$ (the LZM method) [12] with the analyzed FHL method. Weak atomic lines shown in Fig. 2a numbered with *1'*, *2'* and *4'*, *5'*, *6'*, *7'* are practically invisible in the spectra shown in Figs. 2 and 3 in [12]. The fluorescence spectra are formed on the horizontal straight line, whereas, in the LZM method, the peaks of decreased absorption are superimposed on the absorption spectra. This complicates the processing and leads to additional inaccuracies. However, in the LZM method, the peaks of decreased absorption

have the spectral width several times narrower than in the FHL method. Therefore, if in Fig. 2a, in the fields of 1875 and 2500 Gs, component *3* is only partially spectrally resolved, then, in the LZM method, component *3* is fully spectrally resolved (Fig. 3 from [12]).

It was noted above that the SA technique used in [9, 10] to study lines of Rb atoms in external magnetic fields has two significant disadvantages. One of them is the presence of cross-over resonances, which split into numerous components in the magnetic field. In this case, the spectrum becomes extremely difficult to process, which makes it impossible to conduct studies at values of B higher than 100 Gs (it is expected that FHL will be used successfully at fields up to ~1 T). Another disadvantage is that the amplitudes of peaks of decreased absorption do not correspond to probabilities of atomic transitions. This makes the SA method inapplicable for the analysis of changes in transition probabilities in different magnetic fields.

The following control experiment was carried out: as the laser intensity decreases down to 5 mW/cm^2, the spectral width of peak *9* achieved ~70 MHz. One of PMs was set on the table with the micrometer step. In the magnetic field ~2500 Gs, the displacement of PMs by 20 μm (one PM was shifted toward the other) led to the frequency shift of component *9* by 6 MHz to the high-frequency region, which was recorded relatively easily. It is obvious that a nanocell with a furnace can also be fixed on a table with a micrometer step so that the displacements of this system allow one to map strongly inhomogeneous magnetic fields. For the mapping to be more successful, the dimensions of the system (nanocell with furnace) can, in principle, be decreased further; i.e., a conducting and optically transparent deposited layer can replace a furnace and the window thickness can be decreased to 100 μm with the decrease of the transverse dimensions down to several millimeters. The decrease in furnace size will enable the application of higher magnetic fields.

It should be noted that, with regard to sensitivity, the magnetometer based on FHL is far below magnetometers based on coherent processes [1, 2] and optical pumping [18], but has advantages in the measurement of strong and gradient magnetic fields.

CONCLUSIONS

It is shown that the use of the FHL method based on the effect of narrowing of the fluorescence spectrum of a nanocell with the Rb atomic vapor column thickness $L = \lambda/2$ (at optimal parameters, the sevenfold narrowing compared to the Doppler broadening of ~500 MHz) allows the detailed quantitative measurements of both frequency characteristics and probabilities of all 15 atomic transitions between levels of the hyperfine structure $5S_{1/2}$, $F_g = 1 \to 5P_{1/2}$, $F_e = 1, 2$ of ^{87}Rb, $5S_{1/2}$ $F_g = 2, 3 \to 5$ $P_{1/2}$, $F_e = 2, 3$ of ^{85}Rb atoms in magnetic fields ranging within 10–2500 Gs (at the laser σ^+ excitation). For some atomic transitions, as the magnetic field increases, the transition probability increases significantly (more than tenfold), whereas for others it decreases strongly. Advantages of FHL over the existing methods are noted (it is expected that FHL will operate up to 1 T). Small thicknesses of the atomic vapor column (~390 nm) allow the application of PMs, which significantly facilitates the generation of strong magnetic fields. The experimental results are in a good agreement with the theoretical ones.

The results obtained show that the nanocell with the vapor column thickness $L = \lambda/2$ can be used as a basis for a magnetometer with the local spatial resolution ~390 nm, which is important for mapping strongly gradient magnetic fields. The frequency reference shifted by several gigahertz to the high-frequency region relative to the ^{87}Rb transition $F_g = 1 \to F_e = 1$, 2 (D_1 line) can be obtained as well. The both technical applications are rather simple to implement, and in the presence of a nanocell with the thickness $L = \lambda/2$ they can be constructed under laboratory conditions. It should be noted that the FLP method can be used successfully to study D_1 lines of Cs, K, and Na (for Na, the best local spatial resolution can be ~290 nm).

ACKNOWLEDGMENTS

We are grateful to A. Sarkisyan for the nanocell manufacture, A. Papoyan for the useful discussion, and A. Nersisyan and R. Mirzoyan for their technical cooperation.

This work was supported by the ANSEF (grant no. PS1868).

REFERENCES

1. D. Budker, W. Gawlik, D. Kimball, et al., Rev. Mod. Phys. **74**, 1153 (2002).
2. D. Budker, D. F. Kimball, and D. P. DeMille, *Atomic Physics* (Oxford Univ. Press, Oxford, 2004).
3. P. Tremblay, A. Nichaud, M. Levesque, et al., Phys. Rev. A **42**, 2766 (1990).
4. E. B. Aleksandrov, G. I. Khvostenko, and M. P. Chaĭka, *Interference of Atomic States* (Nauka, Moscow, 1991) [in Russian].
5. D. G. Sarkisyan, A. V. Papoyan, T. Varzhapetyan, K. Blush, and M. Auzinsh, Opt. Spektrosk. **96** (3), 373 (2004).
6. D. Sarkisyan, A. Papoyan, T. Varzhapetyan, K. Blush, and M. Auzinsh, J. Opt. Soc. Am. B **22**, 88 (2005).
7. D. Sarkisyan, A. Papoyan, T. Varzhapetyan, J. Alnis, K. Blush, and M. Auzinsh, J. Optics. A **6**, 142 (2004).
8. A. Papoyan, D. Sarkisyan, K. Blush, M. Auzinsh, D. Bloch, and M. Ducloy, Laser Phys. **13**, 1467 (2003).

9. Momeen M. Ummal, G. Rangarajan, and P. C. Deshmukh, J. Phys. **40**, 3163 (2007).
10. G. Skolnik, N. Vujičić, and T. Ban, Opt. Commun. **282**, 1326 (2009).
11. D. Sarkisyan and A. Papoyan, *New Trends in Quantum Coherence and Nonlinear Optics (Horizons in World Physics)*, Ed. by R. Drampyan (Nova Science Publishers, New York, 2009), Vol. 263, p. 85.
12. A. Sargsyan, G. Hakhumyan, A. Papoyan, D. Sarkisyan, A. Atvars, and M. Auzinsh, Appl. Phys. Lett. **93**, 021119 (2008).
13. D. Sarkisyan, D. Bloch, A. Papoyan, and M. Ducloy, Opt. Commun. **200**, 201 (2001).
14. D. A. Steck, http : //steck.us/alkalidata.
15. G. Breit and I. I. Rabi, Phys. Rev. **38** (11), 2082 (1931).
16. J. Alnis and M. Auzinsh, Phys. Rev. A **63**, 023407 (2001).
17. J. Alnis and M. Auzinsh, Eur. Phys. J. D **11** (1), 91 (2000).
18. E. B. Aleksandrov, M. V. Balabas, and V. A. Bonch-Bruevich, Pis'ma Zh. Tekh. Fiz. **13**, 749 (1987).

Translated by A. Gonchar